journal

J. Am. Ceram. Soc., 87 [2] 197–202 (2004)

Zirconia Nanoparticles Made in Spray Flames at High Production Rates

Roger Mueller, Rainer Jossen, and Sotiris E. Pratsinis

Particle Technology Laboratory, Department of Mechanical and Process Engineering, ETH Zurich, CH-8092 Zurich, Switzerland

Mark Watson and M. Kamal Akhtar

Research Center, Millennium Chemicals, Inc., Glen Burnie, Maryland 21060

Synthesis of zirconia nanoparticles by flame spray pyrolysis (FSP) at high production rates is investigated. Product powder is collected continuously in a baghouse filter unit that is cleaned periodically by air-pressure shocks. Nitrogen adsorption (BET), X-ray diffractometry (XRD), transmission electron microscopy (TEM), and thermogravimetric analysis (TGA) are used to characterize the product powder. The effect of powder production rate (up to 600 g/h), dispersion gas flow rate, and precursor concentration on product particle size, crystallinity, morphology, and purity is investigated. The primary particle size of zirconia is controlled from 6 to 35 nm, while the crystal structure consists of mostly tetragonal phase (80–95 wt%), with the balance monoclinic phase at all process conditions. The tetragonal crystal size is close to the primary particle size, which indicates weak agglomeration of single crystals.

I. Introduction

ZIRCONIA (ZrO_2) has a broad range of applications and has become one of the most industrially important ceramic materials of the present time. The traditional applications of ZrO_2 and ZrO_2-containing materials are foundry sands and flours, refractory ceramics, and abrasion resistance materials. Other ZrO_2 applications include catalysts, oxygen sensors, fuel cells, resistive heating elements, and jewelry because of its high oxygen-ion conduction and high refractive index.[1–4] Along with high strength and toughness, ZrO_2 also possesses good hardness, wear resistance, and thermal shock resistance. These properties have led to the use of ZrO_2-based components in many engineering applications, such as automobile engine parts, wire-drawing dies, and cutting tools. The low thermal conductivity and relatively high coefficient of thermal expansion make ZrO_2 a suitable material for thermal barrier coatings on metal components.[2,5]

ZrO_2 particles have been produced by a variety of techniques, including vapor deposition, mechanical milling, laser ablation, flame-based methods, conventional and flame spray pyrolysis, sol–gel methods, and microwave plasma synthesis. The aerosol technology is advantageous, because it does not require the multiple steps, high liquid volumes, and surfactants of wet chemical processes.[6] Fumed tetragonal-phase ZrO_2 particles have been made[7] by evaporating zirconium tetrachloride ($ZrCl_4$) into a hydrogen/air (or oxygen) flame (Aerosil process) consisting of agglomerated primary particles of ~8 nm in diameter. Later, Hartmann *et al.*[8] used the same process and precursor and obtained white and fluffy ZrO_2 powders with average particle diameters between 10 and 50 nm. These particles were of the metastable tetragonal phase with traces of the monoclinic phase. The properties of the fumed oxides were primarily controlled by the flame temperature, which depended on the hydrogen to oxygen ratio. However, the most severe limiting factor of the gas-phase synthesis is the lack of volatility of the starting materials.[7]

Another promising aerosol technology is flame spray pyrolysis (FSP), which overcomes most of the precursor limitations of the gas-phase process. FSP can uniquely fulfill the physical and chemical requirements for synthesis of a broad spectrum of functional nanoparticles in a low-cost, single-step process,[9] because each droplet contains the precursor in the same stoichiometry as desired in the product powder.[10] Nielsen *et al.*[11] made, among other things, up to 5 μm ZrO_2 particles by atomizing a solution consisting of zirconium sulfate ($Zr(SO_4)_2$) and water or alcohol into a natural gas, carbon monoxide, or hydrogen flame. Using FSP, Karthikeyan *et al.*[12] made ZrO_2 consisting of tetragonal as the dominant phase and monoclinic as the minor phase with crystal sizes of 12–21 nm at production rates up to 1.2 g/h. They used zirconium *n*-butoxide ($Zr(C_4H_9O)_4$) in butanol as precursor. Yuan *et al.*[13] used FSP of zirconium *n*-propoxide ($Zr(C_3H_7O)_4$) to make ZrO_2 powders in the micrometer and submicrometer range. These powders consisted of a mixture of tetragonal and monoclinic phases. Laine *et al.*[14] made, among other things, a range of CeO_2/ZrO_2 compositions varying from pure ZrO_2 to pure CeO_2. The specific surface area of these powders was ~10 m^2/g. This system was further investigated by Sutorik and Baliat,[15] who found that, in pure agglomerated ZrO_2 (typical agglomerate size of ~220 nm), the monoclinic phase was dominant, although significant amounts of tetragonal-phase ZrO_2 were also observed. Kilian and Morse[16] used FSP of zirconium *n*-butoxide and zirconium *n*-propoxide to make spherical cubic-phase and monoclinic-phase ZrO_2 at production rates of up to 180 g/h. The particle diameter in these experiments was between 30 and 120 nm. Very recently, Limaye and Helble[17] used FSP of zirconium *n*-butoxide to make tetragonal-phase ZrO_2 particles having mean number diameters ranging from 10 to 90 nm.

However, systematic investigations into the impact of production rate, dispersion gas flow rate, and precursor concentration on ZrO_2 particle characteristics are limited in the above studies. In contrast, Mädler *et al.*[18] systematically studied the effect of oxidant and precursor–solvent composition on the size of silica (SiO_2) primary particles (7–39 nm) at production rates of 12 g/h using FSP. The objective of the present study is to investigate continuous synthesis of crystalline nanostructured ZrO_2 particles by FSP at high production rates in a pilot plant using baghouse filters. Especially, the focus is on the size control of ZrO_2 nanoparticles by varying production rate, precursor concentration, and dispersion gas flow rate.

A. Krell—contributing editor

Manuscript No. 186459. Received December 30, 2002; approved September 26, 2003.

Supported in part by the Swiss National Science Foundation under Grant No. 2100-063632.00/1.

II. Experimental Procedure

(1) Apparatus

Figure 1 shows a schematic of the experimental setup. The spray apparatus consists of a commercially available external-mixing stainless-steel gas-assisted nozzle (Model 970/4-S32, Schlick-Düsen, Gustav Schlick GmbH and Co, Untersieman, Germany) having a capillary tube with an inside diameter of 0.5 mm and an annular gap that can be adjusted to keep a constant pressure drop (1 bar (1×10^5 Pa)) across the nozzle tip regardless of the dispersion gas (>99.95% O_2, PanGas, Zurich, Switzerland) flow rate (25 and 50 L/min). The dispersion gas flow rate is metered by a mass flow controller (Bronkhorst, Ruurlo, the Netherlands). The nozzle is surrounded by two stainless-steel annuluses having inside and outside diameters of 18–19 and 20–25 mm, respectively. These annuluses form a diffusion flame when 2 L/min of methane (>99.5% CH_4, PanGas) flows through the inner annulus and 4.5 L/min of O_2 flows through the outer annulus. These gas flow rates are also metered by mass flow controllers (Bronkhorst). Additional sheath O_2 (15 L/min) is metered by a calibrated rotameter (Vögtlin Instruments AG, Aesch, Switzerland) and fed through a sintered metal plate ring with inner and outer diameters of 28 and 50 mm, respectively, that surrounds the previous outer annulus. Zirconium *n*-propoxide, 70 wt% in *n*-propanol (ChemPur, Karlsruhe, Germany), is used as precursor and is dissolved in ethanol (>99.8% C_2H_5OH, EtOH; Fluka Chemie AG, Buchs SG, Switzerland), which results in precursor solutions of 0.5*M* and 1*M*. The liquid precursor solution feed rate ranges from 6.8 to 81.1 mL/min, which results in ZrO_2 production rates from 50 to 600 g/h. A 1 L precision piston pump (Model 1000D, Isco, Inc., Lincoln, NE) provides a pulsation-free supply of the precursor solution through the capillary tube. Before the particle synthesis is started, an additional syringe pump (Model Syringe Infusion Pump 22, Harvard Apparatus, Holliston, MA) is used for initial heating of the nozzle (Fig. 1) by feeding and burning 5 mL/min of EtOH for 10 min. This helps to assure a constant pressure drop across the nozzle.

Product powders are collected in a commercial jet filter (Model FRR 4/1.2, Friedli AG, Burgdorf, Switzerland) consisting of four polytetrafluoroethylene- (PTFE-, Teflon-) coated baghouse filters (total surface area of 1.7 m^2, Nomex, DuPont, Wilmington, DE), which are cleaned periodically by air pressure shocks. Small samples (~1 g) of product particles are collected with the aid of a vacuum pump (Model RE 16, Vaccubrand GmbH and Co., Wertheim Germany) on a glass-fiber filter (Type GF/A, Whatman, Dietikon, Switzerland) 150 mm in diameter located in a stainless-steel holder that samples the product powder by a bypass connected to the inlet pipe (Fig. 1). Powders collected on the small glass-fiber filter are identical (same specific surface area and morphology) to the powders collected on the baghouse filters.

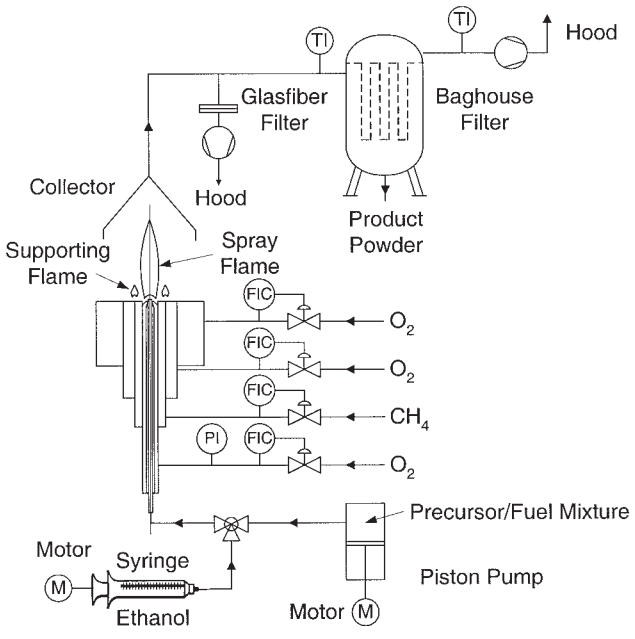

Fig. 1. Schematic of the flame spray pyrolysis (FSP) process for the synthesis of ZrO_2 nanoparticles at high production rates using a commercially available nozzle.

(2) Characterization

The droplet-size distribution is measured by Fraunhofer laser diffraction spectrometry (Model Helos, Sympatec GmbH, Claustal-Zellerfeld, Germany) 5 cm above the nozzle (1 bar pressure drop across the nozzle) in the absence of combustion when pure EtOH is atomized. The droplet mass median diameter is in the range of 10–37 μm. The spray flame height is determined visually as the distance from the nozzle tip to the end of the luminous flame zone.

The powder specific surface area (SSA) is determined from a five-point N_2 adsorption isotherm in the relative pressure range of 0.05–0.25 at 77.3 K (BET analysis; Model Gemini III 2375, Micromeritics Instruments Corp., Norcross, GA). Before the adsorption, the samples are degassed (Model Flow Prep 060, Micromeritics Instruments Corp.) under N_2 atmosphere at 150°C for 1 h, to remove water bound to the particle surface from air moisture. Assuming monodisperse spherical primary particles, the BET-equivalent average primary particle diameter, d_{BET}, is calculated by $d_{BET} = 6/(\rho_p \text{ SSA})$, where ρ_p is the density of tetragonal-phase ZrO_2, 6.1 g/cm^3. Error bars shown in the figures are two times the standard deviation obtained from the results of multiple experiments.

The powder X-ray diffractometry (XRD) spectra are recorded using an advanced diffractometer (Model D8, Bruker Instruments, Billercia, MA) over a 2θ range from 20° to 70°, steps of 0.02°, and a scan speed 0.24°/min. Crystalline characteristics are obtained from the XRD spectra using TOPAS 2.0 software (Model 2000, Bruker AXS) based on the fundamental parameter approach (Rietveld method),[19,20] in which the effects of the equipment (e.g., X-ray source and slits) are incorporated. The crystal size, d_{XRD}, is calculated from the full-width at half-maximum (FWHM) of the peak, using Scherrer's equation,[21] as it is typically done using $d_{XRD} = 0.9\lambda/(\beta \cos \theta)$, where λ is a wavelength of the X-ray (0.154186 nm) and β and θ represent the measured FWHM and a diffraction angle, respectively.

Samples of the product powder are analyzed by transmission electron microscopy (TEM; Model 2000FX II, JEOL, Tokyo, Japan) using an electron microscope operated at 200 kV, with magnifications between 50 and 800 000. The holey carbon-coated copper TEM grids are dipped into the powder, which is collected onto the filter. For each product powder, typically 700–1000 primary particles are counted manually using OPTIMAS 6.51 (Media Cybernetics, Webster, NY) software. Statistical analysis of the data are performed according to Hinds.[22] The composition of the collected powder is determined by thermogravimetric analysis (TGA) in a thermobalance (Model TGA7SDTA851^e, LF/1100°C, Mettler–Toledo, Greifensee, Switzerland) coupled with a mass spectrometer (Model Quadstar 422, Balzers, Liechtenstein). The powder is heated in N_2 from 25° to 120°C at 10°C/min, held at this temperature for 10 min, and then heated at 20°C/min to 800°C and held at this temperature for 10 min. Then, N_2 is replaced by O_2, and the sample is heated at 20°C/min to 1000°C and held there for 5 min.[23,24]

III. Results and Discussion

For all flame spray conditions, only perfectly white ZrO_2 powders are made. The visual indication for carbon-free powders is verified by TGA coupled with mass spectrometry (MS), according to Mueller *et al.*[24] This analysis shows also no indication of remaining carbonaceous species (no weight loss under oxidizing conditions and no CO_2 signal in the MS) in the as-prepared ZrO_2 powders.

(1) Particle Morphology

Representative TEM micrographs of ZrO_2 powders made at 200 g/h using dispersion/oxidant gas flow rates of 25 and 50 L/min and 0.5*M* and 1*M* zirconium *n*-propoxide in EtOH are shown in Fig. 2. The ZrO_2 particles are agglomerated and consist of uniform, spherical primary particles. The BET-equivalent particle diameter of 26 nm (Fig. 2(a)), 20 nm (Fig. 2(b)), 23 nm (Fig. 2(c)), and 14 nm (Fig. 2(d)) are in good agreement with TEM observations. Furthermore, some primary particles stick together by sinter bridges, but they are not fully coalesced, which indicates too low flame temperatures and/or too short residence times of the particles in the high-temperature region. Lattice planes are discernible, which indicates that even the smallest particles are reasonably well crystallized (Fig. 2(a)). Similar ZrO_2 powder morphology was observed by Karthikeyan *et al*.,[12] who showed large agglomerates that consisted of mostly nanosized particles of ~8 nm. Fractal-like agglomerates and nonagglomerated ZrO_2 particles were observed by Limaye and Helble.[17] The formation was dependent on the flame temperature. At low flame temperatures, they observed the formation of nonagglomerated, large ZrO_2 particles, while highly agglomerated fractal-like particles were made at high flame temperatures. Very recently, Kilian and Morse[16] reported the formation of nonagglomerated ZrO_2 particles formed within a size range of 30–120 nm. However, some qualitative TEM pictures were missing.

(2) Particle Size

Figure 3 shows the BET-equivalent average diameter of the ZrO_2 primary particles as a function of the ZrO_2 production rate at two constant dispersion/oxidant gas flow rates of 25 L/min (triangles) and 50 L/min (circles). A dispersion gas flow rate of 50 L/min allows liquid feed rates up to 81.1 mL/min, while, for a dispersion gas flow rate of 25 L/min, the maximum liquid feed rate is 54.1 mL/min. Increasing the liquid feed rate at a constant dispersion gas flow rate decreases the gas to liquid mass ratio (GLMR), which results in an insufficient dispersion of the liquid at too low GLMRs.[25,26]

The zirconium *n*-propoxide concentration in EtOH is 0.5*M* (filled symbols) and 1*M* (open symbols) (Fig. 3). As the liquid feed rate of the 0.5*M* precursor solution is increased from 13.5 to 54.1 or 81.1 mL/min, which corresponds to a ZrO_2 production rate from 50 to 200 or 300 g/h, the particle diameter increases from 12 to 29 nm using a dispersion/oxidant gas flow rate of 25 L/min, while the particle diameter increases from 7 to 26 nm when using an O_2 flow rate of 50 L/min. Likewise, using a precursor concentration of 1*M*,

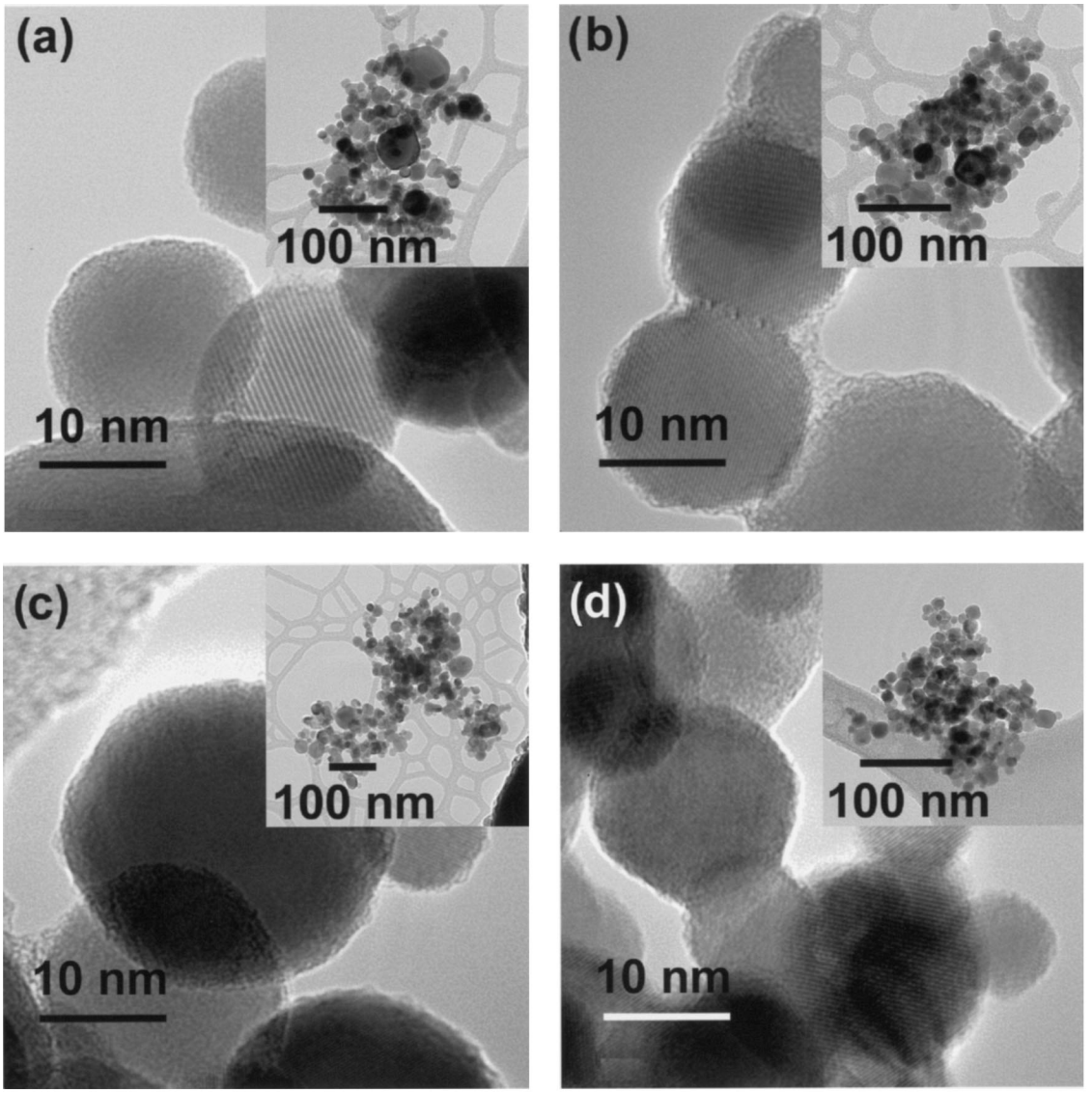

Fig. 2. TEM micrographs of FSP-made ZrO_2 nanoparticles at a production rate of 200 g/h using dispersion gas flow rates of 25 and 50 L/min and 0.5*M* and 1*M* zirconium *n*-propoxide in EtOH at (a) 25 L/min and 0.5*M*, (b) 50 L/min and 0.5*M*, (c) 25 L/min and 1*M*, and (d) 50 L/min and 1*M*.

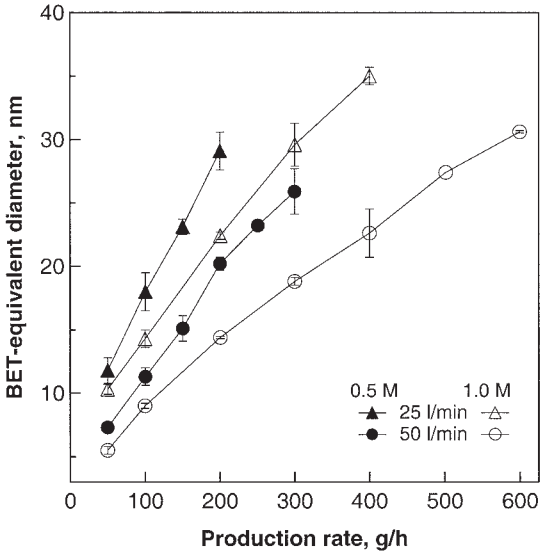

Fig. 3. BET-equivalent diameter of ZrO_2 nanoparticles made by FSP from zirconium *n*-propoxide in EtOH as a function of powder production rate at precursor concentrations of (filled symbols) 0.5*M* and (open symbols) 1*M* and at O_2 dispersion/oxidant gas flow rates of (triangles) 25 L/min and (circles) 50 L/min.

the particle diameter increases from 10 to 35 nm when increasing the liquid feed rate from 6.8 to 54.1 or 81.1 mL/min (production rate from 50 to 400 or 600 g/h) at a dispersion gas flow rate of 25 L/min, while the particle diameter increases from 6 to 31 nm at a dispersion gas flow rate of 50 L/min.

An increase in feed (or ZrO_2 production) rate increases the spray flame height. For example, the flame height increases from 4 to 40 cm when the feed rate of the 1*M* precursor solution increases from 6.8 to 81.1 mL/min, and the dispersion gas flow rate is 50 L/min. The increase in precursor solution feed rate results in higher enthalpy content (from 10.9 to 130 MJ/h at these conditions) of the flame. Hence, the particles have longer residence times at high temperatures. The increase in particle sintering rate at high residence time and high temperature contributes to the formation of larger primary particles. Furthermore, as the zirconium *n*-propoxide concentration increases, the ZrO_2 particle concentration increases. This leads to more particle collisions and, therefore, enhanced particle growth, which increases the particle size, especially when complete coalescence takes place.[27] These results are in agreement with FSP studies of other pure oxides at lower production rates, where an increase of the liquid feed (or production) rate increases the primary particle diameter of Bi_2O_3[28] and CeO_2[29] as well as with SiO_2 formation studies at high production rates using FSP[26] and vapor-fed turbulent hydrogen–air diffusion flames.[23]

Increasing the dispersion/oxidant gas flow rate from 25 to 50 L/min intensifies mixing and accelerates combustion,[30] thus decreasing the spray flame height. The flame height decreases, for example, from 35 to 26 cm when the dispersion gas flow rate increases from 25 to 50 L/min at a 1*M* liquid feed rate of 54.1 mL/min. Additionally, increasing the dispersion gas flow rate decreases the droplet concentration of the spray flame; thus, the particle concentration and the particle residence time at high temperature decrease as the spray flame height decreases. This leads to faster quenching of particle growth and, therefore, smaller particles (Fig. 3). These results are in agreement with other FSP studies.[26,28]

Increasing the precursor concentration from 0.5*M* to 1*M* increases the primary particle diameter. For example, at a liquid feed rate of 40.6 mL/min, the primary particle diameter increases from 23 to 30 nm (corresponding to powder production rates of 150 and 300 g/h, Fig. 3) when increasing the precursor concentration from 0.5*M* to 1*M*. Again, increasing precursor concentration increases the enthalpy content of the flame and mass concentration, and, as a result, the high-temperature particle residence time increases, which favors higher sintering and coagulation rates that result in larger primary and aggregated particles. However, Kilian and Morse,[16] observed the formation of larger particles at more diluted zirconium *n*-butoxide in *n*-butanol solutions, which is in disagreement with the observation in this study.

Most importantly, Fig. 3 shows the operation window for the synthesis of tailor-made ZrO_2 nanoparticles as dispersion gas flow rates lower than 25 L/min result in an insufficient dispersion of the precursor solution, while, at 50 L/min, the exit gap is at its widest opening to maintain a pressure drop across the nozzle tip of 1 bar. Precisely controlled product primary particles can be made by selecting the dispersion gas flow rate (between 25 and 50 L/min) and the precursor concentration at a constant production rate (Fig. 3).

Figure 4 shows the primary particle-size distribution (PPSD) obtained by TEM for ZrO_2 production rates of 100 (triangles) and 300 g/h (circles) using a dispersion gas flow rate of 50 L/min and 0.5*M* zirconium *n*-propoxide in EtOH. The PPSD is shifted to larger average particle diameters as the production rate increases from 100 to 300 g/h (Fig. 4), while the corresponding geometric standard deviation, σ_g, is almost identical (1.64 and 1.63 for the 100 and 300 g/h spray, respectively) but is above 1.45, the self-preserving limit for coagulation.[31] The TEM-counted Sauter mean primary particle diameters, d_s, are 15.3 and 26.7 nm for the 100 and 300 g/h rates, respectively, which are consistent with the corresponding BET-equivalent particle diameters (Fig. 3) of 12.0 nm (100 g/h) and 25.8 nm (300 g/h).

(3) Phase Composition

A representative XRD pattern of ZrO_2 powder made by FSP is shown in Fig. 5. The ZrO_2 is made at a production rate of 200 g/h using a dispersion gas flow rate of 25 L/min and 1*M* zirconium *n*-propoxide in EtOH. The ZrO_2 crystal structure consists of mainly tetragonal (T) phase and limited monoclinic (M) phase. The calculation of d_{XRD} (Scherrer's equation) from the strongest tetragonal-phase peak results in a crystal size of 22 nm, which is in agreement with the BET-equivalent average particle diameter of 23 nm, while the d_{XRD} of the monoclinic structure results in a crystal size of 26 nm. Using the fundamental parameter approach, the phase composition is 95 wt% tetragonal and 5 wt% monoclinic (Fig. 5).

A mixture of mostly tetragonal (85–95 wt%) and monoclinic phases of ZrO_2 is detected by XRD of all FSP-made powders using zirconium *n*-propoxide as precursor. The highest content of tetragonal phase is detected for the smallest ZrO_2 particles, while it decreases slightly with increasing particle diameter. Normally,

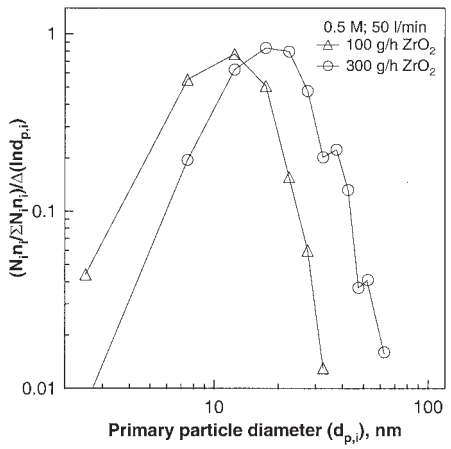

Fig. 4. Primary particle-size distributions of ZrO_2 made at 0.5*M* zirconium *n*-propoxide in EtOH at powder production rates of (△) 100 and (○) 300 g/h using a dispersion gas flow rate of 50 L/min.

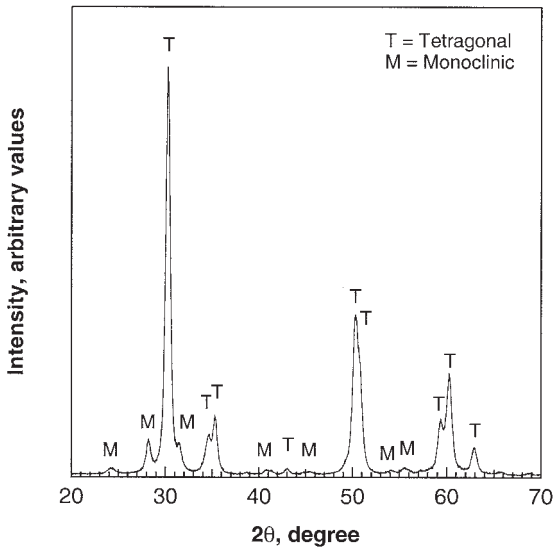

Fig. 5. XRD pattern of ZrO_2 powder made at a production rate of 200 g/h using a dispersion gas flow rate of 25 L/min and 1*M* zirconium *n*-propoxide in EtOH. ZrO_2 crystal structure consists of mainly tetragonal (T, 95 wt%) and monoclinic (M, 5 wt%) phases.

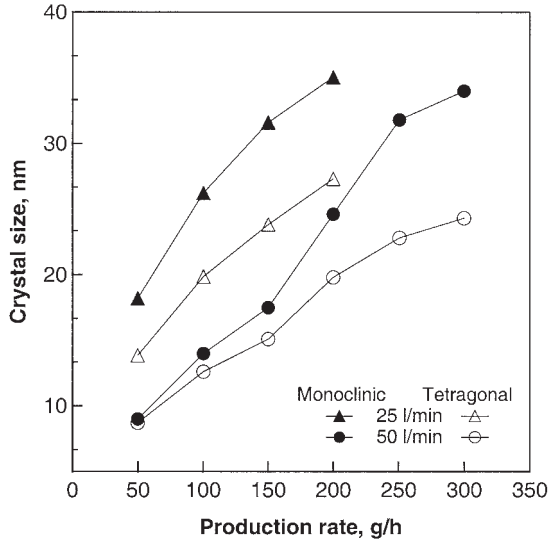

Fig. 6. Crystal size of (filled symbols) monoclinic-phase and (open symbols) tetragonal-phase ZrO_2 made by FSP as a function of the ZrO_2 powder production rate using O_2 dispersion gas flow rate of (triangles) 25 and (circles) 50 L/min at 0.5*M* zirconium *n*-propoxide in EtOH.

ZrO_2 has a monoclinic structure at room temperature and atmospheric pressure, which transforms martensitically to a tetragonal structure at 1170°C and then to a fluorite-type cubic structure at 2370°C.[2,32] The presence of tetragonal-phase ZrO_2 at room temperature can be explained by the Gibbs–Thomson effect. In small particles, the tetragonal structure is energetically favored, while in larger particles, the monoclinic structure is more stable. During the rapid cooling of the nanoparticles, as they flow out of the high-temperature spray flame, the tetragonal structure is quenched. Structural transformation occurs at a critical particle size of 8–18 nm, below which the tetragonal structure is thermodynamically stable.[2,33,34] Formation of tetragonal-phase ZrO_2, even in particles >18 nm (Fig. 5) may result from fast quenching of the particles during FSP. This is in agreement with other FSP studies at much lower production rates[12,13] but is in disagreement with Kilian and Morse,[16] who reported the formation of cubic and monoclinic structures of ZrO_2 particles by FSP without quantifying that phase composition.

Figure 6 shows the average XRD tetragonal (open symbols) and monoclinic (filled symbols) crystal size as a function of the ZrO_2 powder production rate using a dispersion gas flow rate of 25 (triangles) and 50 L/min (circles) at 0.5*M* zirconium *n*-propoxide in EtOH. Both crystal sizes increase with increasing production rate, which is in agreement with Fig. 3, where the BET-equivalent primary particle diameter increases also with increasing powder production rate. Here, the tetragonal crystal size increases from 8.7 to 24.3 nm, while the monoclinic crystal size increases from 9 to 34 nm when increasing the ZrO_2 production rate from 50 to 300 g/h at an O_2 gas flow rate of 50 L/min. Likewise, at 25 L/min O_2 flow rate, the tetragonal crystal size increases from 13.9 to 27.3 nm and the monoclinic crystal size increases from 18.2 to 35.1 nm (powder production rate increases from 50 to 200 g/h). The monoclinic crystal sizes are always larger than the tetragonal crystal sizes produced under the same process conditions. This difference increases with increasing crystal size (higher ZrO_2 production rate) and decreasing dispersion gas flow rate (from 50 to 25 L/min). The fast quenching of the spray flame is more efficient at high dispersion gas flow rates and at low powder production rates. Here, the residence time of the particles in the spray flame is very short, which leads to small primary particles (Fig. 3), where the high-temperature tetragonal phase is quenched in becoming the dominant structure. Longer particle-residence times in the spray flame lead to larger particles, which are quenched more slowly, which results in a decrease of the tetragonal structure and the formation of larger monoclinic crystals (Fig. 6).

The tetragonal crystal sizes (Fig. 6) are astonishingly close to the BET-equivalent particle diameters (Fig. 3), which indicates that the primary particles are weakly agglomerated single crystals. For ZrO_2 powders made at production rates up to 150 g/h, the BET-equivalent particle diameter is slightly smaller than the average tetragonal crystal size. A possible reason for this difference is polydispersity, because the BET-equivalent particle diameter d_{BET} is a surface-weighted particle property, whereas d_{XRD} is a mass-weighted particle property, which leads to $d_{BET}/d_{XRD} < 1$. At higher ZrO_2 production rates (>150 g/h), the d_{BET} is slightly larger than the tetragonal-phase d_{XRD}. Here, the tetragonal-phase content of the powders is slightly lower (down to ~85 wt%), which leads to a larger average crystal size, because monoclinic crystals are, on average, larger than the tetragonal crystals (Fig. 6).

IV. Conclusions

A systematic investigation of flame spray synthesis of ZrO_2 nanoparticles was conducted at high production rates up to 600 g/h using a commercially available external-mixing stainless-steel gas-assisted nozzle. The influence of ZrO_2 powder production rate, precursor concentration, and oxidant dispersion gas flow rate was investigated on the product morphology, average primary particle diameter and size distribution, crystallinity, and purity using 0.5*M* and 1*M* zirconium *n*-propoxide in EtOH. The average particle diameter of pure ZrO_2 was controlled from 6 to 35 nm by varying the production rate, precursor composition, and dispersion gas flow rates. The crystal structure consisted of mostly tetragonal phase (80–95 wt%) and the balance monoclinic phase at all used process conditions. XRD-determined tetragonal crystal sizes were close to the BET-determined primary particle sizes, which indicated that the primary particles were weakly agglomerated single crystals.

References

[1]M. J. Mayo, J. R. Seidensticker, D. C. Hague, and A. H. Carim, "Surface Chemistry Effects on the Processing and Superplastic Properties of Nanocrystalline Oxide Ceramics," *Nanostruct. Mater.*, **11** [2] 271–82 (1999).

[2]T. Chraska, A. H. King, and C. C. Berndt, "On the Size-Dependent Phase Transformation in Nanoparticulate Zirconia," *Mater. Sci. Eng. A-Struct. Mater. Prop. Microstruct. Process.*, **286** [1] 169–78 (2000).

[3]M. Gell, "Application Opportunities for Nanostructured Materials and Coatings," *Mater. Sci. Eng. A-Struct. Mater. Prop. Microstruct. Process.*, **204** [1–2] 246–51 (1995).

[4]H. Gleiter, "Materials with Ultrafine Microstructures: Retrospectives and Perspectives," *Nanostruct. Mater.*, **1** [1] 1–19 (1992).

[5]R. Nielsen and T. W. Chang, "Zirconium and Zirconium Compounds"; pp. 543–67 in *Ullmann's Encyclopedia of Industrial Chemistry*, Vol. A28. Wiley–VCH Verlag, Weinheim, Germany, 1996.

[6]S. E. Pratsinis and S. V. R. Mastrangelo, "Material Synthesis in Aerosol Reactors," *Chem. Eng. Prog.*, **85** [5] 62–66 (1989).

[7]A. T. Liu and P. Kleinschmit, "Production of Fumed Oxides by Flame Hydrolysis"; pp. 1–10 in *Novel Ceramic Fabrication Processes and Applications*, Vol. 38. Edited by R. W. Davidge. Institute of Ceramics, Staffs, U.K., 1986.

[8]W. Hartmann, A. T. Liu, D. Peuckert, and P. Kleinschmit, "Fumed Oxides as Base Materials for Ceramic Applications," *Mater. Sci. Eng. A-Struct. Mater. Prop. Microstruct. Process.*, **109**, 243–46 (1989).

[9]H. K. Kammler, L. Mädler, and S. E. Pratsinis, "Flame Synthesis of Nanoparticles," *Chem. Eng. Technol.*, **24** [6] 583–96 (2001).

[10]G. L. Messing, S. C. Zhang, and G. V. Jayanthi, "Ceramic Powder Synthesis by Spray Pyrolysis," *J. Am. Ceram. Soc.*, **76** [11] 2707–26 (1993).

[11]M. L. Nielsen, P. M. Hamilton, and R. J. Walsh, "Ultrafine Metal Oxides by Decomposition of Salts in a Flame"; pp. 181–95 in *Ultrafine Particles*. Wiley, New York, 1963.

[12]J. Karthikeyan, C. C. Berndt, J. Tikkanen, J. Y. Wang, A. H. King, and H. Herman, "Nanomaterial Powders and Deposits Prepared by Processing of Liquid Precursors," *Nanostruct. Mater.*, **8** [1] 61–74 (1997).

[13]F. L. Yuan, C. H. Chen, E. M. Kelder, and J. Schoonman, "Preparation of Zirconia and Yttria-Stabilized Zirconia (YSZ) Fine Powders by Flame-Assisted Ultrasonic Spray Pyrolysis (FAUSP)," *Solid State Ionics*, **109** [1–2] 119–23 (1998).

[14]R. M. Laine, T. Hinklin, G. Williams, and S. C. Rand, "Low-Cost Nanopowders for Phosphor and Laser Applications by Flame Spray Pyrolysis"; pp. 500–510 in *Metastable, Mechanically Alloyed, and Nanocrystalline Materials*, Parts 1 and 2, Vols. 343–346. TransTech Publications, Zurich-Uetikon, Switzerland, 2000.

[15]A. C. Sutorik and M. S. Baliat, "Solid-Solution Behavior of $Ce_xZr_{1-x}O_2$ Nanopowders Prepared by Flame Spray Pyrolysis of Solvent-Borne Precursors"; pp. 371–76 in *Metastable, Mechanically Alloyed and Nanocrystalline Materials*, Vols. 386–388. TransTech Publications, Zurich-Uetikon, Switzerland, 2002.

[16]A. Kilian and T. F. Morse, "A Novel Aerosol Combustion Process for the High Rate Formation of Nanoscale Oxide Particles," *Aerosol Sci. Technol.*, **34** [2] 227–35 (2001).

[17]A. U. Limaye and J. J. Helble, "Morphological Control of Zirconia Nanoparticles through Combustion Aerosol Synthesis," *J. Am. Ceram. Soc.*, **85** [5] 1127–32 (2002).

[18]L. Mädler, H. K. Kammler, R. Mueller, and S. E. Pratsinis, "Controlled Synthesis of Nanostructured Particles by Flame Spray Pyrolysis," *J. Aerosol. Sci.*, **33** [2] 369–89 (2002).

[19]R. W. Cheary and A. Coelho, "A Fundamental Parameters Approach to X-ray Line-Profile Fitting," *J. Appl. Crystallogr.*, **25**, 109–21 (1992).

[20]R. W. Cheary and A. A. Coelho, "Axial Divergence in a **C**onventional X-ray Powder Diffractometer. I. Theoretical Foundations," *J. Appl. Crystallogr.*, **31**, 851–61 (1998).

[21]R. C. Rau, "Routine Crystallite-Size Determination by X-ray Diffraction Line Broadening," *Adv. X-ray Anal.*, **5**, 104–15 (1962).

[22]W. C. Hinds, *Aerosol Technology*; pp. 75–110. Wiley, New York, 1999.

[23]H. K. Kammler, R. Mueller, O. Senn, and S. E. Pratsinis, "Synthesis of Silica–Carbon Particles in a Turbulent H_2–Air Flame Aerosol Reactor," *AIChE J.*, **47** [7] 1533–43 (2001).

[24]R. Mueller, H. K. Kammler, K. Wegner, and S. E. Pratsinis, "OH Surface Density of SiO_2 and TiO_2 by Thermogravimetric Analysis," *Langmuir*, **19** [1] 160–65 (2003).

[25]A. H. Lefebvre, *Atomization and Sprays*; pp. 201–72. Taylor and Francis, London, U.K., 1989.

[26]R. Mueller, L. Mädler, and S. E. Pratsinis, "Nanoparticle Synthesis at High Production Rates by Flame Spray Pyrolysis," *Chem. Eng. Sci.*, **58** [10] 1969–76 (2003).

[27]S. E. Pratsinis, "Flame Aerosol Synthesis of Ceramic Powders," *Prog. Energy Combust. Sci.*, **24** [3] 197–219 (1998).

[28]L. Mädler and S. E. Pratsinis, "Bismuth Oxide Nanoparticles by Flame Spray Pyrolysis," *J. Am. Ceram. Soc.*, **85** [7] 1713–18 (2002).

[29]L. Mädler, W. J. Stark, and S. E. Pratsinis, "Flame-Made Ceria Nanoparticles," *J. Mater. Res.*, **17** [6] 1356–62 (2002).

[30]I. Glassman, *Combustion*; pp. 1–34. Academic Press, San Diego, CA, 1996.

[31]S. Vemury and S. E. Pratsinis, "Self-Preserving Size Distributions of Agglomerates," *J. Aerosol. Sci.*, **26** [2] 175–85 (1995).

[32]R. C. Garvie, "The Occurrence of Metastable Tetragonal Zirconia as a Crystallite Size Effect," *J. Phys. Chem.*, **69** [4] 1238–43 (1965).

[33]R. Ramamoorthy, D. Sundararaman, and S. Ramasamy, "X-ray Diffraction Study of Phase Transformation in Hydrolyzed Zirconia Nanoparticles," *J. Eur. Ceram. Soc.*, **19** [10] 1827–33 (1999).

[34]G. Skandan, "Processing of Nanostructured Zirconia Ceramics," *Nanostruct. Mater.*, **5** [2] 111–26 (1995). □